frontiers | Frontiers in Environmental Science

ORIGINAL RESEARCH
published: 27 June 2022
doi: 10.3389/fenvs.2022.887425

Adsorption of Methyl Orange and Cr (VI) Onto Poultry Manure-Derived Biochar From Aqueous Solution

Usman Ghani[1†], Wenjia Jiang[2†], Kiran Hina[1*], Atif Idrees[3], Meenal Iqbal[1], Muhammad Ibrahim[4], Rashid Saeed[1], M. Kashif Irshad[4] and Imran Aslam[5]*

[1]Department of Environmental Sciences, Faculty of Science, University of Gujrat, Gujrat, Pakistan, [2]School of Safety and Environment, Fujian Chuanzheng Communications College, Fuzhou, China, [3]Guangdong Key Laboratory of Animal Conservation and Resource Utilization, Guangdong Public Laboratory of Wild Animal Conservation and Utilization, Institute of Zoology, Guangdong Academy of Sciences, Guangzhou, China, [4]Department of Environmental Sciences, Government College University Faisalabad, Faisalabad, Pakistan, [5]Department of Basic Sciences and Humanities, University of Engineering and Technology Lahore, Lahore, Pakistan

OPEN ACCESS

Edited by:
Zahoor Ahmad,
The University of Haripur, Pakistan

Reviewed by:
Muhammad Idrees,
Shenzhen University, China
Farhat Abbas,
University of Prince Edward Island, Canada

***Correspondence:**
Kiran Hina
kiran.hina@uog.edu.pk
Wenjia Jiang
jiangwenjia23@163.com

[†]These authors have contributed equally to this work

Specialty section:
This article was submitted to Soil Processes, a section of the journal Frontiers in Environmental Science

Received: 01 March 2022
Accepted: 26 April 2022
Published: 27 June 2022

Citation:
Ghani U, Jiang W, Hina K, Idrees A, Iqbal M, Ibrahim M, Saeed R, Irshad MK and Aslam I (2022) Adsorption of Methyl Orange and Cr (VI) Onto Poultry Manure-Derived Biochar From Aqueous Solution. Front. Environ. Sci. 10:887425. doi: 10.3389/fenvs.2022.887425

In recent years, heavy metals and other organic compound pollution has increased and become a considerable global problem due to its direct impacts on the aquatic ecosystem. This study is aimed to see how efficient the poultry manure-derived biochar is in removing chromium (VI) and methyl orange simultaneously from the aqueous solutions through adsorption. Chromium present in the form of reactive ions such as $HCrO_4^-$ and $Cr_2O_7^{2-}$ at pH 2–6 values and in stable form, CrO_4^- at alkaline pH. In this study, biochar was synthesized by the slow pyrolysis of feedstock in a muffle furnace at 550°C temperature with 2 mm particle size. This study provided the biochar with S_{BET} 16.0921 m^2/g rough stomata-like pores with a volume of 0.0074 cm^3/g, pore diameter 1.84 nm, aromatic groups, and structural diversity. A batch adsorption experiment was conducted to investigate the adsorption efficiency, and mechanism was elucidated by fitting isotherm and kinetic models and result analysis along with the thermodynamics. From the linear Langmuir fit results the maximum adsorption capacity (q_{max}) of biochar reached up to 20.8 and 19.09 mg g^{-1} for MO and Cr, respectively. Different operational factors like reaction time, pollutant initial concentration, effect of temperature, and sorbent material dose were studied at pH 4 and initial concentration of 100 mg/L using 2 g of the adsorbent dose. The linear Langmuir well fitted with the experimental data having R^2 value of 0.99 and 0.99 for MO and Cr, respectively. From the obtained results, the highest adsorption efficiency reached 88.80% and 90.231% for MO and Cr, respectively.From kinetics study, non-linear pseudo–second-order (PSO) model are highly fitted with the obtained data with R^2 of 0.97 and 0.974 for MO and Cr, respectively. The result analysis revealed that $HCrO_4^-$ and $Cr_2O_7^{2-}$ ions compete with the SO_3^- to attach on the surface of the sorbent which leads to competitive adsorption of Cr (VI) and MO onto BC. Thermodynamic study presents that the change in Gibbs free energy ΔG° is negative, indicates that the whole process was favorable and completed. The adsorption process was monolayer physisorption, irreversible, and endothermic. Hence, it can be said that this material is environmental friendly and an economical sorbent for high adsorption efficiency.

Keywords: poultry manure biochar, pyrolysis, isotherms, adsorption efficiency, soil pollution

INTRODUCTION

Around the globe, water pollution has increased due to the organic and inorganic pollutant disposal. Wastewater is a worldwide and fundamental issue because it has direct effects on the aquatic ecosystems and is being increased at a higher ratio due to overpopulation (Cosgrove and Loucks, 2015). It comes from many sources like agriculture and industry; most of the elements in the water come from industries such as textile, pesticides, and fertilizers that are washed from crops and farms (Mateo-Sagasta et al., 2017). Dyes are considered as highly toxic as they may pose negative threats to the biota and human health. Methyl orange (MO) and many other dyes are widely used in the textile, paper, printing, culinary, and pharmaceutical sectors. Dyes have been digested and converted into aromatic amines by intestinal bacteria (Ismail et al., 2019; Jawad et al., 2019) cause, high toxicity (carcinogenicity and teratogenicity), and make stable complex aromatic molecular structure (Wang et al., 2015). Chromium (Cr) is a trace metal that may be found in most natural settings; it has two oxidation states as trivalent chromium (Cr (III)) and hexavalent (Cr (VI)); the former is an important micronutrient (Shang et al., 2014). Hexavalent chromium (Cr (VI)) is the most prevalent oxidized form of Cr and is considered as water soluble; it produces highly reactive oxyanions (Mishra and Bharagava, 2016), which cause toxicity to biological cells. Cr (III), on the other hand, is known to generate very stable and insoluble OH^- precipitates and is hence considered chemically inert. Hexavalent chromium exists in the ionic form of $HCrO_4^-$ and $Cr_2O_7^{2-}$ at pH values 2–6 and is instable and reactive, whereas in alkaline pH, it exists in the form of CrO_4^- and is stable. The Cr (VI) concentration in the environment is frequently caused by anthropogenic activity. Many industries dispose chromium into the water resources, especially released during polishing, tanning, metal plating, and other processes (Jaishankar et al., 2014).

Wastewater treatment processes mainly include the adsorption processes (Li et al., 2016), photocatalysis (Yang et al., 2014), membrane separation, and biological and chemical oxidation (Donkadokula et al., 2020). Although many techniques and methods has been devised and are used to treat MO and Cr individually (Lu et al., 2016), only few studies have focused on the synergistic removal of MO and Cr due to their diverse physicochemical properties. Although, mechanism chemistry for synergistic removal has been reported previously (Gholami et al., 2020; Qiu et al., 2020), among all, the adsorption is still preferred because of its simplicity, low cost, and efficacy (Karimi-Maleh et al., 2021). So far, many commercial sorbent materials for dyes and heavy metal removal are available such as activated carbon and zeolite material, but this research still has lower adsorption efficiency results, secondary pollution production, higher production cost, and instable chemical nature which pose a serious challenge for the removal of Cr (VI) and MO (Kyzas et al., 2015; Jung et al., 2016). Recently, hexavalent chromium and other pollutant adsorption has been studied and interpreted as there is a competitive adsorption process occurring as Cr (VI) compete with other pollutants for adsorption on material surfaces (Cheng et al., 2021).

Therefore, the production of a material with higher adsorption capacity, stable chemical nature, and economically and environmentally friendly for the synergistic removal of Cr (VI) and MO is urgently needed (Wang et al., 2020). Recently, biochar has received special attention as adsorbents due to its renewability, environmental friendliness, and low-cost and is being extensively employed for the synergistic removal of organic and inorganic pollutants from wastewaters. BC have higher carbon contents and can be prepared by using the standard pyrolysis method under anerobic conditions at a high temperature. Since BC has large surface area, abundant functional groups, and porous structure to adsorb organic pollutants on its surface, it is, therefore, important to make biochar based on pollutants' relevancy for the protection of the environment (Kang et al., 2019). However, low binding capacity of the anionic and cationic pollutants may affect their pragmatic use due to the limited ion exchange capacity. Therefore, surface modification of BC and new material biosorbents may open new horizons for the efficient removal of MO and Cr (Premarathna et al., 2019).

In this study, biochar was prepared by the slow pyrolysis of poultry manure at higher temperature and examined as an effective sorbent for the synergistic removal of MO and Cr (VI) from aqueous solutions. To evaluate the optimized conditions, various experiments were conducted such as the sorbent material dose, reaction time, pH, effect of temperature, and pollutant initial concentration. The mechanism of the adsorption process was investigated by fitting the isotherm and kinetic models and analysis of experimental results. The thermodynamics study was also performed to check the reaction chemistry. It was hypothesized that by using this poultry manure-derived biochar, the adsorption efficiency will be higher at optimized conditions.

MATERIALS AND METHODS

Chemicals, Equipment, and Apparatus

High purity and analytical grade chemicals and reagents ($K_2Cr_2O_7$, NaOH, HCl, and ethanol), purchased from Shalimar Scientific Store, Pakistan, were used in this study. All glassware like conical flasks were washed with distilled water before use, and an adsorption experiment was performed using 500-ml Erlenmeyer conical flasks on the shaker (Orbi-Shaker™) filled with 250 ml of solution; the pH of the working solutions was adjusted using 0.1 M HCl/NaOH and measured by using a pH multimeter (pHTestr® # Z-527831). The concentrations of methyl orange and chromium were calculated from the calibration curve using absorbance data by UV-visible spectroscopy (Genesys 20 spectrophotometer) at 540 and 460 nm wavelengths using the 1.5-diphenylcarbazide method.

Synthesis of the Adsorbent and Characterization

Semi-dried poultry manure was collected from a poultry farm in Rawalpindi, Pakistan. Poultry manure samples were semi-

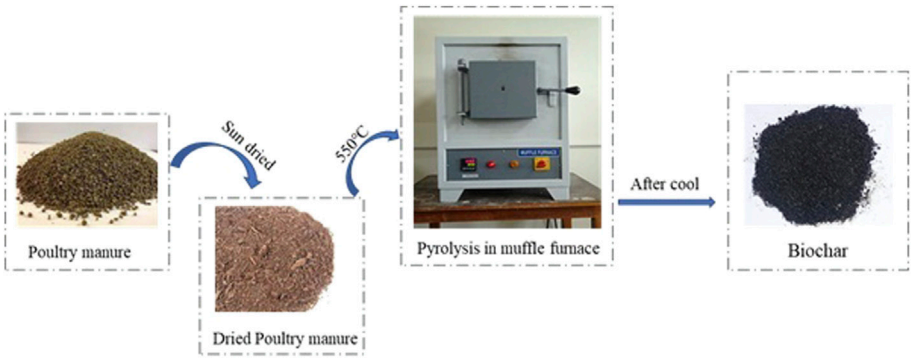

FIGURE 1 | Synthesis of the poultry manure biochar (PMB).

decomposed in the botanical garden, University of Gujrat, Gujrat, Pakistan. Afterward, the oven-dried samples were passed through a sieve to produce a required particle size. The crushed material was taken into alumina crucible, covered with an aluminum sheet, then placed in a muffle furnace (Thermo Scientific™ FB1310M), was programed at 550°C for 3 h at a ramping rate of 10°C/min, and then, the crucible was left to cool. The final material was washed using ethanol and DI water, dried at 105°C overnight. The obtained yield of biochar was packed in an airtight plastic zip-lock bag and was later used in adsorption (**Figure 1**). The prepared carbonaceous materials (poultry manure biochar) were characterized by various advanced techniques. The structural properties were analyzed by using a scanning electron microscope (SEM; Hitachi S-3000N, Hitachi Scientific Instruments, Tokyo, Japan, and surface functional groups) and identified by Fourier transform infrared spectroscopy (Model: FTIR Spectrum 100 PerkinElmer) at the spectral range of 4,000–400 cm^{-1}. The Brunauer–Emmett–Teller (BET) surface area and pore size of the prepared biochar were analyzed by N_2 adsorption–desorption isotherms at 77 K using a Micromeritics (ASAP 2020; Norcross, GA, United States) analyzer.

Adsorption Experiments

To study the adsorption efficiency, a series of batch experiments were conducted using 250 ml of working solution in 500-ml volume conical flasks at neutral pH except for analyzing the effect of pH. The working solution was prepared by dissolving methyl orange powder and $K_2Cr_2O_7$ in deionized water. To evaluate the effect of adsorbent dosage, (1–3 g) sorbent with 100 mg/L pollutant concentration working solution was shaken in an orbital shaker at 125 rotations per minute agitation speed for 120 min at room temperature. Following the same way, a series of experiments were conducted using working solution with pH of 4, 5, 5.5, 6, 6.5, 7, 7.5, 8, and 9 adjusted with 0.1 M HCl/NaOH reagent to analyze its effect. For the time effect, the mixture was withdrawn at the desired interval (0–180 min) and afterward placed in centrifugation tubes at 1,000 rpm, and later, the supernatant was filtered using a 0.45-μm PVDF filter and analyzed by UV-Vis spectroscopy for adsorption efficiency. To investigate the effect of temperature, different experiments were conducted at 298, 303, 313, and 323 K temperature and analyzed for removal efficiency using 150 mg/L pollutant concentration at neutral pH and 2 g adsorbent dose for 120 min. In a similar mode, experiments were conducted with a different initial concentration of pollutants from 10 to 300 mg/L. For the reusability test experiment, 1 g of BC with pollutant loadings was mixed with 30 ml of the 0.1 M HCl/NaOH reagent; after centrifugation, the solution was filtered, and the concentration was analyzed in solution after desorption.

The maximum adsorption capacity and efficiency used as indicators for overall adsorption performance and removal efficiency were calculated using **Eq. 1** and the maximum adsorption capacity qe (mg/g) from **Eq. 2**, where Ci and Ce correspond to initial and final concentrations of pollutants (mg/L), respectively. V indicates the working solution volume (L), and m is the sorbent quantity.

$$\%R = \frac{(Ci - Ce)}{Ci} \times 100, \tag{1}$$

$$qe = \frac{(Ci - Ce) \times V}{m}. \tag{2}$$

RESULTS AND DISCUSSION

Characterization

The surface structural properties of biochar have been investigated by scanning electron microscopy, and it has a rough surface with a scar-like heterogeneous structure (**Figures 2A–D**). This scar-like surface of the poultry manure biochar had a high porosity structure (**Figure 2A**), but the surface of BC was uneven and char-deposited (**Figures 2C,D**). Moreover, there are many large stomata-like pores and attachment sites on the surface of BC (**Figure 2D**), which corresponds to high surface area due to volatilization of organic matter in biomass. With the increasing surface area, the adsorption capacity also increases (Jin et al., 2018; Coleman et al., 2019).

The structure of the prepared biochar was analyzed by N_2 adsorption isotherms. S_{BET} was calculated from N_2 adsorption at

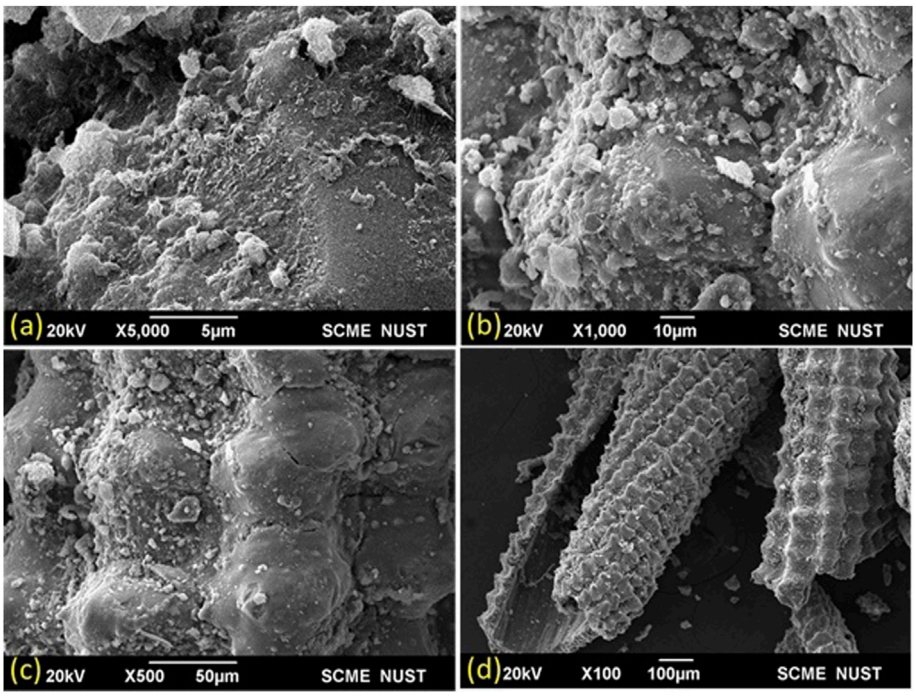

FIGURE 2 | SEM (Scanning electron microscopy) images of the prepared poultry manure biochar. **(A)** 5000, **(B)** 1000, **(C)** 500, **(D)** 100.

77 K using the Brunauer–Emmett–Teller (BET) method. However, the other physical properties such as pore volume and pore size are listed in **Table 1**, indicating that poultry manure-derived biochar has S_{BET} 16.0921 m^2/g and pore size 1.84 nm from the BET method. The plot of the adsorption isotherm, pore volume distribution, and BET surface area are given in **Figure 3**. The experimental results indicate that poultry manure-derived biochar comprises micropores completely, which means it has a microporous structure. The volatilization of organic matter caused micropores in biochar. Generally, particles with size <2 nm diameter are microporous, 2–50 nm range mesoporous, and >50 nm are known as macroporous structures.

The surface structural properties and functional groups were identified by Fourier transform infrared (FTIR) spectra. The biochar is used as an adsorbent material for treating wastewater as a high surface area and hole-like structure can perform an essential role in surface adhesion of methyl orange and chromium (Nguyen and Oh, 2019). The IR spectra of the poultry manure-derived biochar are shown in **Figure 4**. The IR spectra of PMB represent that it has diverse functional groups across the different ranges of absorption peaks. The strong peak between 3,500 and 3,300 cm^{-1} appeared after adsorption was assigned as the –OH group compared to before adsorption. The C=C double bond referred to the absorption peak at 1,630 cm^{-1} after adsorption and the peak strength reduced at pyrolysis temperature of 550°C compared to the previous study of Zolfi Bhovariani et al. (2019) at a lower temperature biochar. The weak peak was found at 1,406 cm^{-1}, which was changed to 1,412 cm^{-1} after adsorption assigned to $-CH_2$ based on the aldehyde group. The strength of the peak was enhanced due to higher sorption of pollutants. Moreover, the peak between 1,000 and 1,100 cm^{-1} was known as the deformed C–O bond. The double conjugated bond C=O appeared at 1,650 and 1,500 cm^{-1} (Mahamad et al., 2015). The band at 870 cm^{-1} is C–H bond vibration in aromatic compounds; this peak vanished after adsorption, and vibration between 700 and 800 cm^{-1} has been assigned as the C–H bond in hetero-aromatic compounds (Lustosa Filho et al., 2017; Daramy et al., 2020). A weak absorption peak between 450 and 700 cm^{-1} corresponds to Si–O–Si.

Effect of Time

The contact time between the sorbent and adsorbate is a critical parameter in the adsorption process to evaluate the capacity of the prepared sorbent; it gives information about how much time is needed for the maximum adsorption of the pollutant which can help in developing wastewater treatment. To evaluate the time effect, a series of experiments were conducted under different times of contact (from 0–180 min), at same conditions of 2 g/L adsorbent dose, neutral pH, and at room temperature in an orbital shaker under 125 rpm of agitation speed. The results of the contact time effect are shown in **Figure 5D**. The calculated values of removal efficiency for MO and Cr were 85.48 % and 88.5%, respectively, and the adsorption capacities qe were 10.68 and 11.06 mg g^{-1} for MO and Cr, respectively. As the time increased from 40 to 120 min, the removal rate increased rapidly to maximum 85.48 % and 88.5% from 47.9 % and 48.35% for MO and Cr, respectively, and further contact did not catalyze the efficiency. It is conferred that the removal efficiency of methyl orange and chromium increased as the

TABLE 1 | Physical characteristics of the poultry manure-derived biochar.

[a]S_{BET} (m^2/g)	[b]$S_{(external)}$ (m^2/g)	[c]S_{mic} (m^2/g)	[d]Total pore volume (cm^3/g)	[e]Micropore volume(cm^3/g)	[f]BET pore diameter (nm)	[g]BJH pore diameter (nm)	[h]DFT pore diameter(nm)
16.0921	15.0791	1.0130	0.007412	0.000345	1.84232	2.6	2.734

[a]*surface area from the BET method.*
[b]*external surface area from the t-plot method.*
[c]*micropore surface area from the t-plot method.*
[d]*total volume calculated from the N_2-adsorbed amount at p/p = 0.25.*
[e]*micropore volume from the t-plot method.*
[f]*pore diameter from the BET method.*
[g]*pore diameter from the Barret–Joyner–Hanlenda (BJH) method.*
[h]*pore diameter from the DFT method.*

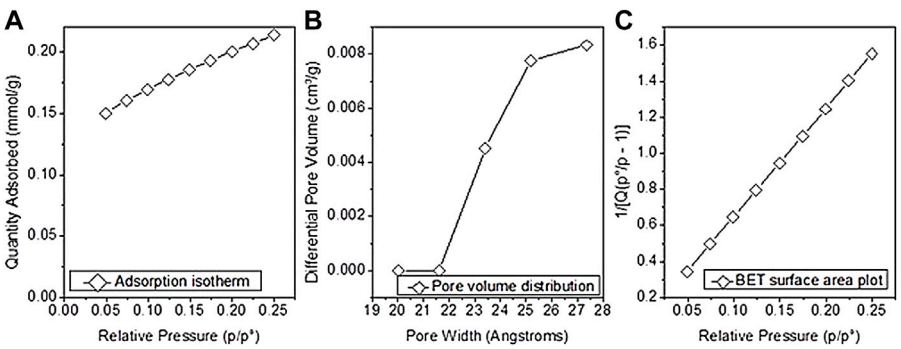

FIGURE 3 | N_2 adsorption isotherms. **(A)** Pore volume distribution **(B)** and BET surface area plot **(C)**.

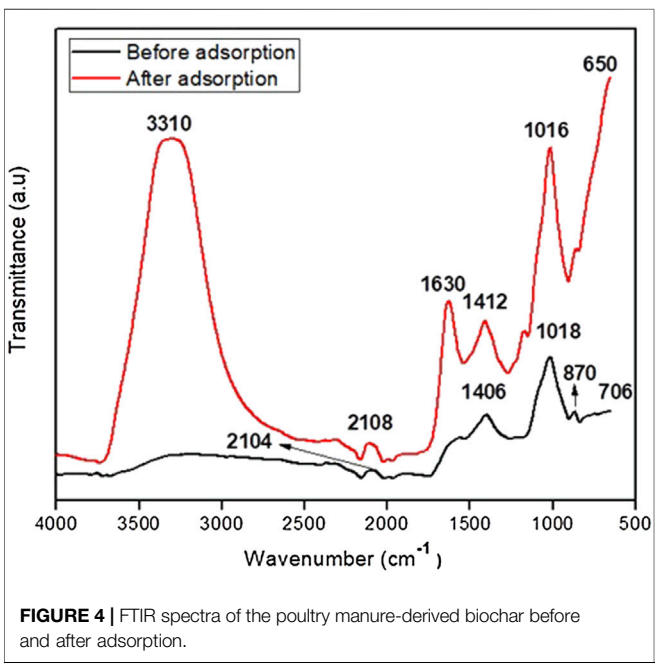

FIGURE 4 | FTIR spectra of the poultry manure-derived biochar before and after adsorption.

time of contact increased and then became stable reaching at 120 min to validate the results in the literature. Liu et al., (2020) confirmed that the adsorption capacity of polyethyleneimine-modified corncob biochar increased for removing MO and Cr synergistically as the contact time increased. The adsorption reached to an equilibrium stage when 120 min of contact time passed, and the values of removal efficiencies were described earlier. Upon elucidating the results, it was seen that maximum sorption occurred rapidly in the first 120 min, and these data were used for kinetic study, as discussed in the adsorption kinetics section. Generally, it is known that increasing contact time have an impact on getting high adsorption rate but up to a limit because active sites on the surface of biochar become saturated, and no further adhesive behavior was showed by the sorbent (Coleman et al., 2019; Jang and Kan, 2019). Thus, based on the experimental results, the optimum contact time for the conducted study was 80 min for the maximum adsorption efficiency.

Effect of Adsorbent Dose

The quantity of the added dose of the sorbent has significant effect on the adsorption capacity investigated and is shown in **Figure 5A**. The removal of MO and Cr was seen to increase as the sorbent dose increased. In the experimental work, adsorbent dosages of 1, 1.5, 2, 2.5, and 3 g were used. The maximum removal reached to 79.17 % and 74.54% for MO and Cr at 2.5 g. Increasing the dose further does not improve the removal, while according to the results of Ghorbani-Khosrowshahi and Behnajady (2016), by increasing the adsorbent dose to 0.4 g from 0.2 g, the adsorption rate also increased. The improvement in removal referred to high attachment sites on the BC surface, and

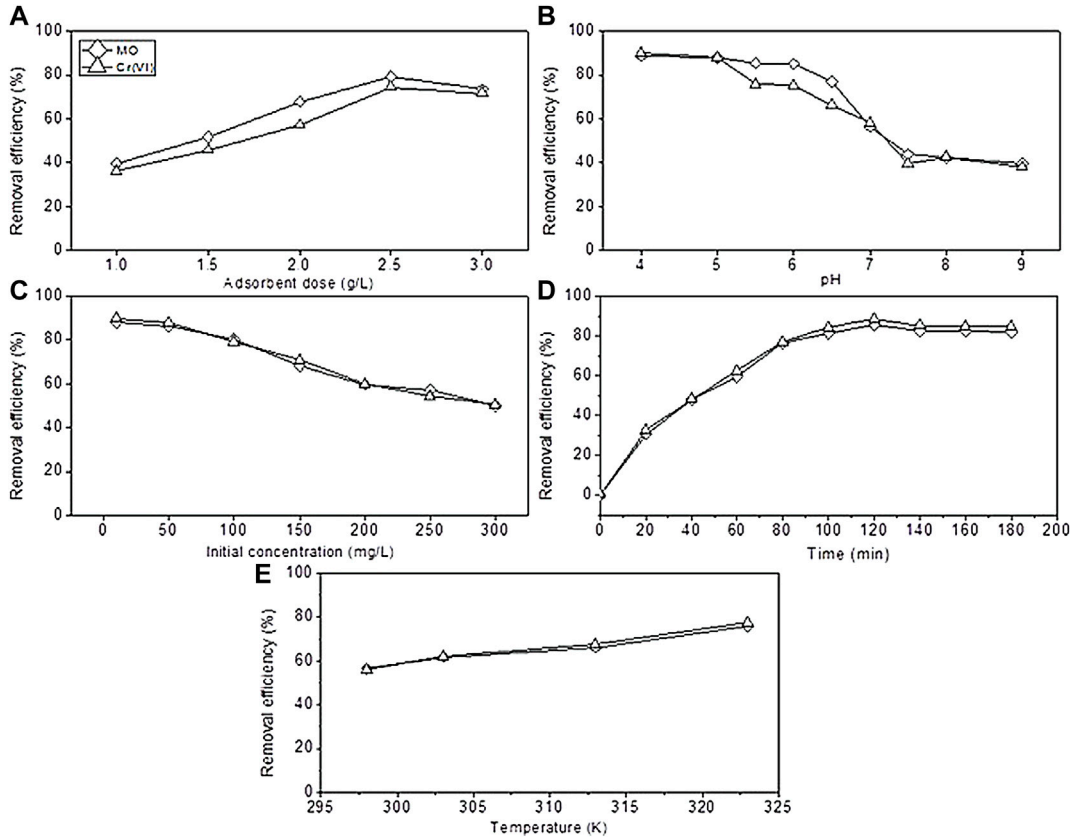

FIGURE 5 | Effect of operational parameters. **(A)** Adsorbent dose, **(B)** pH, **(C)** initial concentration, **(D)** time, and **(E)** temperature.

driving force initially caused diffusion of pollutants to the biochar surface (Pan et al., 2016; Bardestani et al., 2019; Sun et al., 2019). Adding more adsorbent did not improve the efficiency of MO and Cr removal due to surface saturation between the adsorbed ions and solution. On the basis of the obtained results, the optimized dose of the sorbent was considered to be 2.5 g. Other studies conducted by Cheng et al., (2021) confirmed that the efficiency improved from 36.4 to 93.3% as the dose increased toward 4 g of the sorbent.

Effect of pH

In **Figure 5B**, the pH effect on the efficiency of MO and Cr removal is shown. A series of experiments conducted across the range of 4.0–9.0 to delineate the pH dependence of the adsorption process and other factors remain fixed. The results revealed that the PMB adsorption efficiency was maximum at 88.80 % and 90.23% for MO and Cr, respectively, at the acidic pH. As it becomes alkaline, the efficiency decreases to 39.88 % and 38.19% at 9.0 pH, respectively, and the results by Dong et al., (2021) showed that the capacity of adsorbent material reached the maximum in acidic pH. This could be due to surface species on the adsorbent surface. Therefore, the optimal pH for higher results is found to be 4.0. The pH nature has a significant effect on the functional groups of sorbent materials. The high efficiency at the acidic pH may be described by the presence of H^+ ions and charge of the sorbent material, which have significant impact on the electrostatic interaction of the sorbent material with the pollutant molecule (Alshameri et al., 2014). The literature reported that acidic pH between 2 and 6 Cr exists in the form of $HCrO_4^-$ and $Cr_2O_7^{2-}$, which can be rapidly adsorbed onto the BC surface by an electrostatic interaction because the solution has H^+ ions; so it increases the attraction between the sorbent and adsorbate material. Acidic pH causes protonation of the sorbent surface functional groups which resulted in high electrostatic interaction. At the alkaline pH conditions, deprotonation of the surface functional groups occurs, which means that there is a higher density of OH^- ions, thereby indicating that higher negative charges on the surface of the sorbent material might affect the pollutant molecules to attach and induce competition of adsorption for CrO_4^{2-}. Moreover, it produces electrostatic repulsion among similarly charged ions which resulted in lower adsorption. The removal rate of Cr (VI) decreases as the pH of a working solution becomes alkaline pH, as reported by Dong et al., (2017). The main redox reactions in the adsorption mechanism are as follows:

$$Cr_2O_7^{2-} + H_2O \rightarrow 2HCrO_4^-, \quad (3)$$

$$HCrO_4^- \rightarrow CrO_4^{2-} + H^+, \quad (4)$$

$$2CrO_4^{2-} + 2H^+ \rightarrow Cr_2O_7^{2-} + H_2O, \quad (5)$$

$$Cr2O_7^{2-} + 14H^+ + 6e^- \rightarrow 2Cr^{3+} + 2H_2O, \quad (6)$$

$$CrO_4^{2-} + 4H_2O + 3e^- \rightarrow Cr(OH)_3 + 5OH^-. \quad (7)$$

Effect of Initial Concentration

The initial concentration of the working solution has significant effect on the removal of MO and Cr, so a series of experiments were conducted using 10–300 mg/L concentrations (**Figure 5C**). According to the results, highest efficiency reached to 87.94% and 89.87% for MO and Cr, respectively, at 10 mg/L, and when the concentration of 300 mg/L was used, the efficiency become low reaching 50.034% and 50.45% for MO and Cr, respectively. These results supported by the study of Ghorbani-Khosrowshahi and Behnajady (2016) indicated that an increase in the initial concentration impacted the adsorption efficiency to decrease. These results could be described as at a low pollutant concentration, there is a high surface area, and attachment sites are present to attach the large number of molecules, which resulted in high efficiency, while the efficiency decrease as the pollutant concentration become high. This occur because of the competition among molecules to attach on the restricted surface of the sorbent material (Oh and Seo, 2016). Many previous studies reported that the saturated pollutant concentration caused reduction in the overall efficiency due to the attachment competition on the sorbent material (Kang et al., 2019).

Effect of Temperature

Figure 5E showed the effect of temperature on the adsorption of MO and Cr. In this work, a series of experiments were conducted at 298, 303, 313, and 323 K temperature using the 150 mg/L initial concentration and 2 g adsorbent dose at neutral pH for 120 min. From the experimental results, increase in temperature improved the removal efficiency. When the temperature increased from 298 to 323 K, the removal efficiency reached to 76.02% and 77.57% from 56.47% and 56.05% for MO and Cr, respectively. These results indicated that an increase in temperature of the adsorption reaction may increase the kinetic energy of $Cr_2O_7^{2-}$ and SO_3^- ions to the biochar's affinity level, which leads to active attachment of both the pollutants on the BC surface, and the endothermic adsorption process occurred, and this description can be supported by (Cheng et al., 2021).

Isotherms Study

Langmuir, Freundlich, and Tempkin models were plotted for isotherm studies by Origin Pro 8.1 (Origin Lab, United States); nonlinear (**Eqs 8**, **11**, **13**) and linear (**Eqs 9**, **12**, **13**) forms of models are given in the following equations.

The Langmuir equation is as follows:

$$qe = \frac{qmK_LCe}{1 + K_LCe}, \quad (8)$$

$$\frac{1}{\mathrm{qe}} = \frac{1}{K_L\mathrm{qmax}}.\frac{1}{\mathrm{Ce}} + \frac{1}{\mathrm{qmax}}, \quad (9)$$

$$R_L = \frac{1}{1 + K_L.Ce}. \quad (10)$$

The Freundlich equation is as follows:

$$qe = KfCe^{1/n}, \quad (11)$$

$$\mathrm{Logqe} = \mathrm{Log\,Kf} + \frac{1}{\mathrm{n}}\mathrm{LogCe}. \quad (12)$$

The Tempkin equation is as follows:

$$qe = \frac{RT}{bT}lnaTCe, \quad (13)$$

$$\mathrm{qe} = \frac{\mathrm{RT}}{\mathrm{bT}}\mathrm{lnAT} + \left(\frac{\mathrm{RT}}{\mathrm{bT}}\right)\mathrm{lnCe}. \quad (14)$$

In the aforementioned equations, q_{max} indicates the monolayer sorption capacity (mg/g), Langmuir constant K_L (L/mg) describes the affinity of the adsorbent toward the adsorbate, and R_L is the separation factor, while in the Freundlich linear equation, Kf corresponds to the Freundlich constant (mg/g or L/mg) which quantifies the adsorption strength, n is the adsorption intensity parameter, the Tempkin model has the AT binding constant (L/g), bT indicates the Tempkin constant, and R indicates the universal gas constant (8.314 J/mol/K) at T temperature of 298 K.

All the values of the parameters of linear and nonlinear fitting of isotherm models are shown in **Table 2**. The Freundlich plot logCe vs. logqe, Langmuir plot 1/Ce vs. 1/qe, and a plot of lnCe against qe for the Tempkin isotherm model and nonlinear fitting are given in **Figures 6A–D**, respectively. The values of maximum adsorption capacity (q_{max}) R_L and R^2, calculated by the Langmuir model, are presented in **Table 2**. The correlation coefficient (R^2) of MO and Cr from the linear Langmuir model was considerably higher ($R^2 \geq 0.99$; ≥0.99) than that of both the Freundlich ($R^2 \geq 0.932$; ≥0.935) and Tempkin models ($R^2 \geq 0.97$; ≥0.977). The coefficient value for the Freundlich isotherm was less than the Tempkin model. According to both the linear and nonlinear fitting, the best fit of the Langmuir model indicated that monolayer physical sorption occurred, and it better described the MO and Cr adsorption on PMB (**Figure 6B**). When seen, the heterogeneity constant (1/n) values from the Freundlich model were 0.564 and 0.536 for MO and Cr, respectively (if 1/n = 1 means linear adsorption, 1/n > 1 chemical sorption, and 1/n < 1 physical favorable adsorption take place) (Zeng et al., 2019). Another important parameter R_L was calculated to evaluate using **Eq. 10**; the adsorption efficiency and the value of separation factor R_L were 0.177 and 0.139 for MO and Cr, respectively, which meant that sorption is favorable (when R_L is 0, it indicates irreversible, and when it is great than 0 and less than 1, it means sorption is favorable, and when it is equal to unity, it is the linear form of sorption). The pollutants being adsorbed produces the monolayer on the surface of the sorbent material, and it becomes limited. When all the attachment sites are filled, no more adsorption occurred. The Langmuir model fit best with the sorbent which has limited surface attachment sites (Huang et al., 2016; Coleman et al., 2019). The maximum adsorption capacities (q_{max}) derived from the linear fit

TABLE 2 | Adsorption isotherm model parameters' values.

Adsorbent	Pollutant	Linear fitting of isotherm models									
PMB		Langmuir				Freundlich			Tempkin		
		q_{max} (mg/g)	K_L	R_L	R^2	Kf	1/n	R^2	BT (J/mol)	KT (L/mg)	R^2
	MO	20.8	0.046	0.177	0.999	1.358	0.564	0.932	3.26	0.813	0.97
	Cr	19.09	0.061		0.139	0.999	1.525	0.536	0.935	3.12	1.019	0.977
Nonlinear fitting of isotherm models											
		Langmuir				Freundlich			Tempkin		
		q_m (mg/g)	KL		R^2	Kf	1/n	R^2	BT (J/mol)	KT(L/mg)	R^2
	MO	20.8	0.04		0.98	2.62	0.4	0.96	0.834	3.71	0.97
	Cr	20.33	0.046		0.97	2.83	0.38	0.97	1.01	3.524	0.977

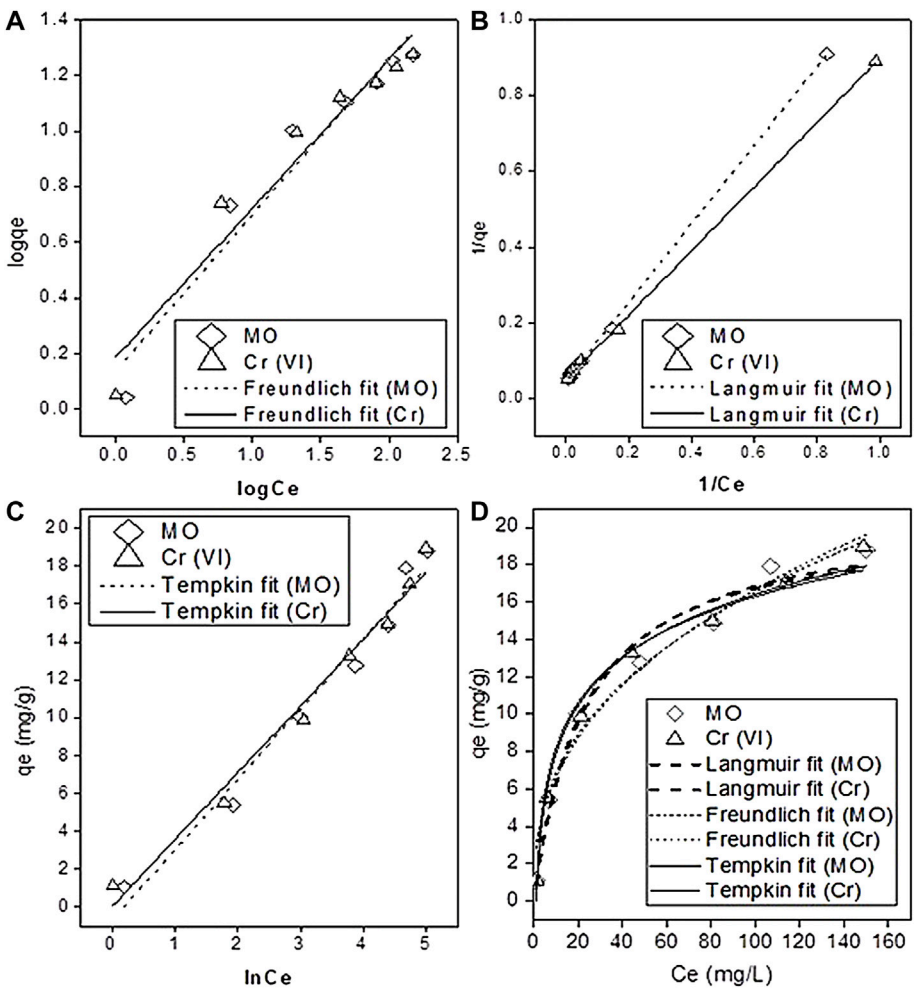

FIGURE 6 | Adsorption isotherms. **(A)** Freundlich, **(B)** Langmuir, **(C)** Tempkin isotherm model, and **(D)** nonlinear isotherm models.

Langmuir model for MO and Cr were 20.8 and 19.09 mg g^{-1}, respectively, and the nonlinear fitting derived values are 20.8 and 20.33 mg g^{-1}, respectively.

Adsorption Kinetics

The adsorption kinetics of methyl orange (MO) and chromium (VI) were analyzed by fitting the kinetic models and calculating

the correlation coefficient R^2 values to check the higher fitting of the model.

The linear and non-linear pseudo–first-order is as follows:

$$\ln(qe - qt) = \ln(K_1 qe) - K_1 t, \tag{15}$$

$$\mathrm{qt} = \mathrm{qe}(1 - \exp^{-\mathrm{KLt}}). \tag{16}$$

The linear and nonlinear pseudo–second-order is as follows:

$$\frac{t}{qe} = \frac{1}{K_2 qe^2} + \frac{t}{qe}, \tag{17}$$

$$qt = \frac{K_2.qe^2.t}{1 + K_2.qe.t}. \tag{18}$$

Generally, the pseudo–first-order (PFO) state, the initial stage of the adsorption process, and the pseudo second-order model (PSO) are applied for the understanding of the whole adsorption process based on the adsorption capacity. The linear and nonlinear forms of both the models are presented in **Eqs. 15–18**. The plot fit of the nonlinear and linear pseudo–first-order and pseudo–second-order models are given in **Figures 7A–D**. From the experimental data, the value of K_1 was acquired from the slope method of the linear plot of ln (qe-qt) vs. t, and the values of K_2 and *qe* were determined by the slope of the linear plot of t/qt vs. t. (**Figures 7C,D**). The nonlinear pseudo second-order model is highly fitted with the experimental data with a high correlation coefficient R^2 value of 0.97 and 0.974 for MO and Cr, respectively, than PFO as compared to nonlinear fitting (**Figure 7D**). The values of K_2 are 71.37 and 57.49 for MO and Cr, respectively (Dhiman and Kondal, 2021). These fitting results suggested that closed chemisorption occurs, which involve electron sharing between the pollutant and biochar. All the detailed values of other important parameters of the kinetic models are presented in **Table 3**.

Thermodynamics Study

The reaction temperature has significant effect on the adsorption efficiency. In this work, the adsorption experiment was conducted in temperature from 298–323 K and analyzed its effects on the adsorption process by calculating the thermodynamic parameters like change in Gibbs free energy change ΔG°, heat of enthalpy ΔH°, and reaction entropy ΔS° change. The values of all the thermodynamic parameters are presented in **Table 4**, and the Van't Hoff plot is given in **Figure 9**. The Gibbs free energy change was calculated using the Van't Hoff **Eq. 19**

$$\Delta G^{\circ} = -\mathrm{RTln}K_c, \tag{19}$$

$$K_C = \frac{Ci - Ce}{Ce}. \tag{20}$$

Here, R represents the universal gas constant, T is the temperature, and Kc is the thermodynamic equilibrium constant (calculated using **Eq. 20**). Moreover, ΔH° and ΔS° are calculated from the slope method using **Eq. 21**.

$$\ln K_c \frac{\Delta S^{\circ}}{R} - \frac{\Delta H^{\circ}}{RT}. \tag{21}$$

All the values of ΔG° of both the pollutants are negative, which indicate that the adsorption process was spontaneous and favorable at higher temperature. The value of change in heat of enthalpy of the adsorption reaction greater than 0 means the adsorption is endothermic, and irreversible reaction occurred. These values exceeding the range of physical adsorption heat values (8.37–62.8 KJ/mol) correspond that chemical sorption occurs as the hexavalent chromium reduced to trivalent chromium (Yu et al., 2018). The values of ΔS° are also greater than 0, which indicate that the arbitrary movement of ions occurred and the freedom of degree of pollutants increased with temperature (Guo et al., 2020). These results confirmed that the whole adsorption process was endothermic and favorable at high temperature.

Adsorption Mechanism

In the literature, adsorption is a widely used method to treat dye and heavy metals from the aqueous solution, isotherm, and kinetic modeling being used primarily to investigate the mechanism of adsorption. To delineate the adsorption mechanism of MO and Cr onto the biochar isotherm, the kinetic models were applied, and the important parameters were calculated. **Tables 2**, **3** showed the values of all important parameters. According to the experimental fitted data, the mechanism followed the pseudo–second-order kinetic model which corresponds to the adsorption of MO and Cr *via* the chemisorption method, involving the covalent interactions between the pollutant and surface functional groups (–OH, –COOH, and C=O) because electrons were shared to Cr (VI) for the reduction to Cr (III) form, whereas the Langmuir model highly conform the data which indicate the physical sorption of MO and Cr. From the results, optimum conditions for high adsorption of both the pollutants was found to be acidic pH of 4.0 because of higher electrostatic attraction between the pollutant and biochar surface. At an acidic condition, the surface charge and protonation of the surface functional groups enhance the adsorption capacity. The oxygen-containing functional groups such as –OH and Si–O–Si provide electrons to hexavalent chromium and reduce it to trivalent chromium ions, which may be released into the working solution.

From the FTIR results, it can be seen that the presence of oxygen-containing functional groups attracts more $HCrO_4^-$ and $Cr_2O_7^{2-}$ compared to SO_3^- of MO and electrostatic affinity of $HCrO_4^-$ and $Cr_2O_7^{2-}$ toward functional groups, which is higher (Mahamad et al., 2015). Guo et al., (2020) reported that the reduction of hexavalent chromium to trivalent chromium is an electron sharing process under acidic conditions due to presence of hydroxyl and aromatic functional groups. Thus, following this mechanism, a following reduction path **Eqs 22**, **23** may occur.

$$\mathrm{R - OH_2^+ + HCrO_4^- \rightarrow R - OH_2CrO_4^- + H^+}, \tag{22}$$

$$HCrO_4^- + 3e^- + 7H^+ \rightarrow Cr^{3+} + 4H_2O. \tag{23}$$

After the adsorption process, a peak appeared at 3,310 and 870 cm^{-1}, while the peak 2,104 cm^{-1} slightly shifted to 2,108 and 1,406 cm^{-1} to 1,412, 1,018 to 1,016 cm^{-1}, and 706 cm^{-1} to 650 cm^{-1}, respectively.

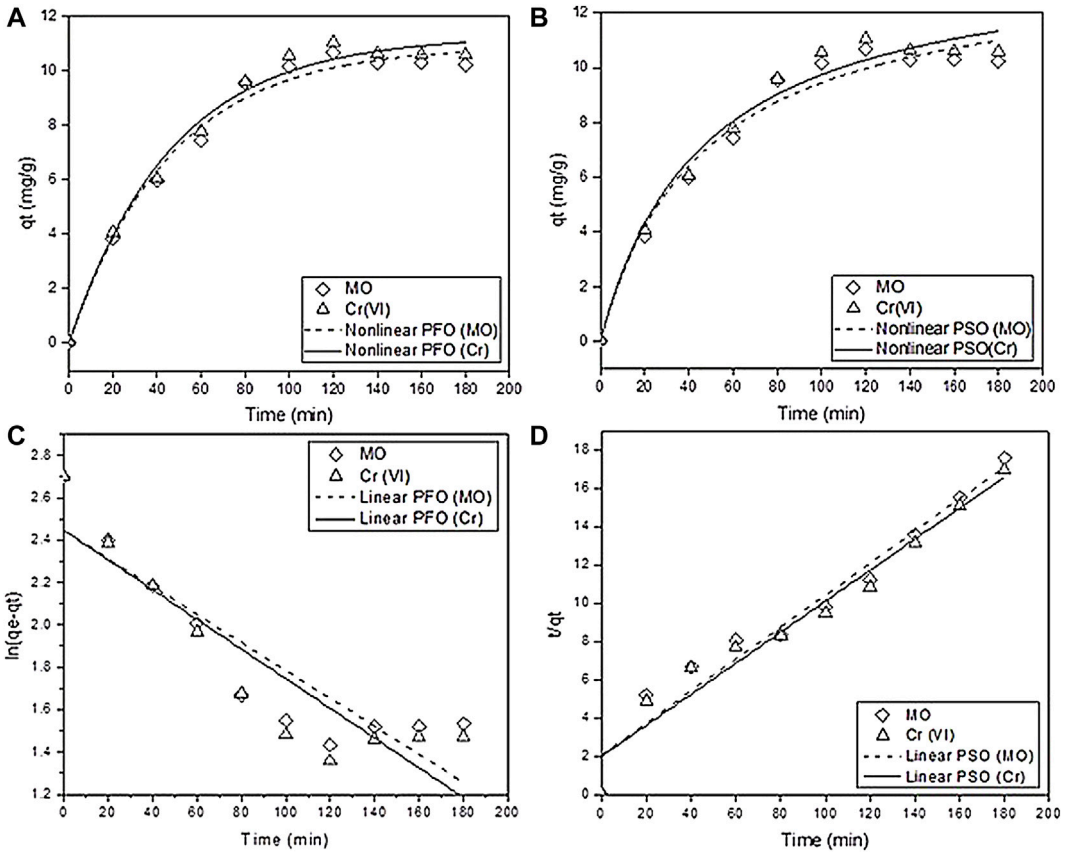

FIGURE 7 | Kinetic adsorption models. **(A)** NLPFO, **(B)** NLPSO, **(C)** LPFO, and **(D)** LPSO.

TABLE 3 | Pseudo–first-order and pseudo–second-order kinetic model parameter values.

Adsorbent PMB	*LPFO			LPSO			
	q_e (mg/g)	K_1	R^2	q_e (mg/g)	qe^2 (mg/g)	K_2	R^2
MO	11.53	−3.67E-05	0.788	11.95	142.87	68.72	0.951
Cr	11.55	−3.89E-05	0.798	12.33	152.33	75.55	0.952
	NLPFO			**NLPSO**			
	q_e (mg/g)	K_1	R^2	q_e (mg/g)	qe^2 (mg/g)	K_2	R^2
MO	10.91	0.0217	0.98	13.80	190.44	0.00154	0.97
Cr	11.27	0.0216	0.98	14.26	203.34	0.00151	0.974

** LPFO and LPSO = Linear pseudo–first-order and linear pseudo–second-order*

*** NLPFO and NLPSO = Nonlinear pseudo–first-order and nonlinear pseudo–second-order*

TABLE 4 | Thermodynamic parameters of pollutants onto the poultry manure-derived biochar.

Adsorbent	Pollutant	Temp. (K)	K_c	$-\Delta G^\circ$ (KJmol^{-1})	ΔH° (KLmol^{-1})	ΔS° (JK^{-1}mol^{-1})	R^2
PMB	MO	298	0.260	0.645	26.98	92.67	0.945
		303	0.481	1.214			
		313	0.674	1.755			
		323	1.154	3.099			
	Cr	298	0.243	0.603	30.32	103.75	0.960
		303	0.492	1.240			
		313	0.730	1.901			
		323	1.240	3.332			

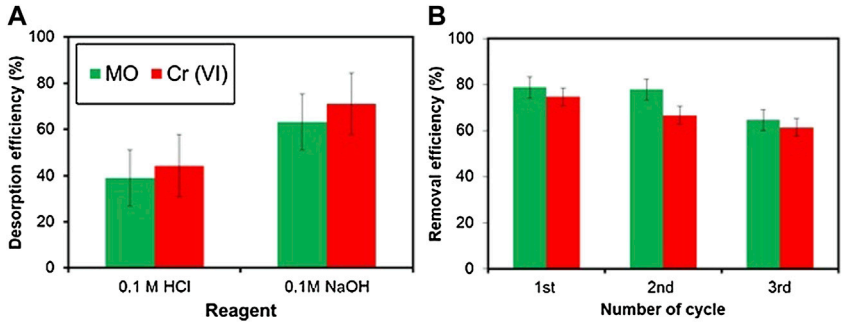

FIGURE 8 | Desorption efficiency **(A)** and reusability test **(B)**.

Re-Usability Test

Reusability of an adsorbent is an important property as the prepared sorbent proved high adsorption efficiency for MO and Cr simultaneously. The desorption efficiency of the two reagents is shown in **Figure 8A**, in which 0.1 M NaOH had a higher efficiency than 0.1 M HCl, which reached up to 63.095 % and 71.037% for MO and Cr, respectively. Hence, 0.1 M NaOH was used as the desorbing agent, and the BC was reused for adsorption again. **Figure 8B** showed the number of reusability cycles of the poultry manure biochar after being desorbed using 0.1 M HCl, for the removal of MO and Cr using 100 ml of solution. The biochar was reused for three cycles after desorption. The efficiency of the sorbent decreased by 6.5%, 7.59%, and 23.3% for MO and 5.9%, 16%, and 22.75%, for Cr, respectively after the 1st, 2nd, and 3rd cycle compared to the adsorption efficiency before the desorption experiment, while in the study of Liu et al., (2020), the efficiency of the adsorbent decreased up to 3% after reuse. These results proved the good reusability of the prepared poultry manure-derived sorbent. The desorption efficiency was calculated according to **Eq. 23**.

$$\%\text{Desorption} = \frac{(V_d \times C_d)}{(C_i - C_e)} \times 100.$$

In the aforementioned equation, Vd indicates the desorbing agent volume (ml), Cd is the concentration of the pollutant after desorption (mg/L), and Ci and Ce are the initial and final concentrations of the pollutant after adsorption (mg/L), respectively.

CONCLUSION

This study provided the BC with a higher specific surface area, diverse aromatic groups, and structural roughness. The specific surface area 16.09 m^2/g, porosity 0.0074 cm^3/g, pore diameter 1.84 nm, and aromaticity of BC were all positively associated with the adsorption efficiency. The unavailability of active sites on the BC surface might partially justify all-time low adsorption capacity. The poultry manure biochar arises as a good adsorbent in MO and Cr removal as the percentage of removal is more than 88.80% and 90.23%, respectively, at 100 mg/L initial concentration and pH 4. Different operational parameters that affect the adsorption capacity were investigated, such as the effect of time,

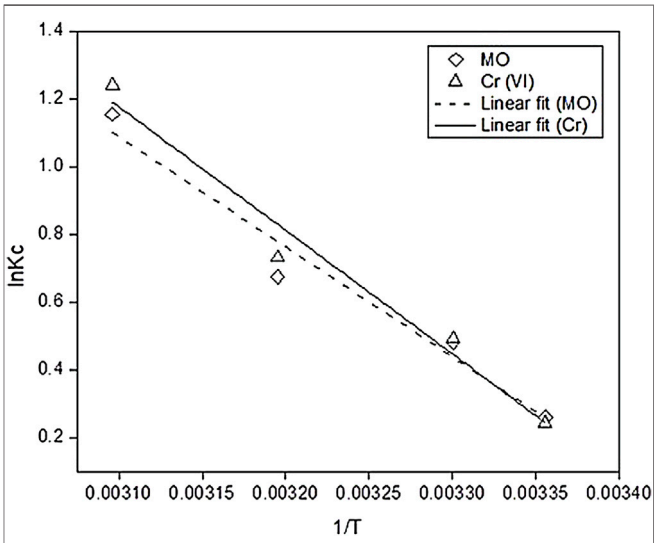

FIGURE 9 | Van't Hoff plot for the calculation of thermodynamics parameters.

dose, pH, and pollutant initial concentration. Upon observing the results, the adsorption efficiency decreased with the increase in the initial concentration. As the concentration increased from 10 mg/L to 300 mg/L, the efficiency decreased from 87.94% and 89.87% to 50.03 % and 50.45% for MO and Cr, respectively. With the increasing contact time, the efficiency of MO and Cr increased more than 85% and 88% up to 120 min and reached to a limit after the efficiency decreased. The Langmuir model highly fitted with the experimental data, and R^2 values of the Langmuir model were 0.999 and 0.999 for MO and Cr, respectively. The fitting results of the adsorption kinetics revealed that pseudo–second-order best fitted to data with R^2 values of 0.94 and 0.974 for MO and Cr, respectively. The surface functional groups attracted the $HCrO_4^-$ and $Cr_2O_4^{2-}$ ions than MO which resulted in the competitive adsorption onto the biochar surface. The change in Gibbs free energy is negative, which indicates that the adsorption process was favorable, spontaneous, and complete. The other thermodynamic parameters ΔH° and ΔS° are positive, which correspond toward the reaction and is endothermic. Hence, the poultry manure-derived biochar is a potential candidate for removing MO and Cr simultaneously from aqueous solutions.

DATA AVAILABILITY STATEMENT

The raw data supporting the conclusion of this article will be made available by the authors, without undue reservation.

AUTHOR CONTRIBUTIONS

Conceptualization, UG, KH, and AI. Data curation, MeI and MuI. Formal analysis, RS, MKI, and MuI. Funding acquisition, MuI and WJ. Methodology, UG, KH, and AI. Project administration, IA. Software, MeI and MKI. Validation, RS. Writing—original draft, UG and KH. Writing—review and editing, MuI and WJ. All authors have read and agreed to the published version of the manuscript.

FUNDING

This research study was funded by the Educational and Scientific Program of Young Teacher, Department of Education, Fujian Province (No. JAT210709), Fujian Chuanzheng Communications College Science and Education Development Fund Doctor Research Launch Special (No.202201109).

REFERENCES

Alshameri, A., Ibrahim, A., Assabri, A. M., Lei, X., Wang, H., and Yan, C. (2014). The Investigation into the Ammonium Removal Performance of Yemeni Natural Zeolite: Modification, Ion Exchange Mechanism, and Thermodynamics. *Powder Technol.* 258, 20–31. doi:10.1016/j.powtec.2014.02.063

Bardestani, R., Roy, C., and Kaliaguine, S. (2019). The Effect of Biochar Mild Air Oxidation on the Optimization of Lead(II) Adsorption from Wastewater. *J. Environ. Manag.* 240, 404–420. doi:10.1016/j.jenvman.2019.03.110

Cheng, H., Liu, Y., and Li, X. (2021). Adsorption Performance and Mechanism of Iron-Loaded Biochar to Methyl Orange in the Presence of Cr6+ from Dye Wastewater. *J. Hazard. Mater.* 415, 125749. doi:10.1016/j.jhazmat.2021.125749

Coleman, B. S. L., Easton, Z. M., and Bock, E. M. (2019). Biochar Fails to Enhance Nutrient Removal in Woodchip Bioreactor Columns Following Saturation. *J. Environ. Manag.* 232, 490–498. doi:10.1016/j.jenvman.2018.11.074

Cosgrove, W. J., and Loucks, D. P. (2015). Water Management: Current and Future Challenges and Research Directions. *Water Resour. Res.* 51, 4823–4839. doi:10.1002/2014wr016869

Daramy, M. A., Kawada, R., and Oba, S. (2020). Alterations of the Chemical Compositions, Surface Functionalities, and Nitrogen Structures of Cage Layer Chicken Manure by Carbonization to Improve Nitrogen Bioavailability in Soil. *Agronomy* 10, 1031. doi:10.3390/agronomy10071031

Dhiman, V., and Kondal, N. (2021). ZnO Nanoadsorbents: A Potent Material for Removal of Heavy Metal Ions from Wastewater. *Colloid Interface Sci. Commun.* 41, 100380. doi:10.1016/j.colcom.2021.100380

Dong, F.-X., Yan, L., Zhou, X.-H., Huang, S.-T., Liang, J.-Y., Zhang, W.-X., et al. (2021). Simultaneous Adsorption of Cr(VI) and Phenol by Biochar-Based Iron Oxide Composites in Water: Performance, Kinetics and Mechanism. *J. Hazard. Mater.* 416, 125930. doi:10.1016/j.jhazmat.2021.125930

Dong, H., Deng, J., Xie, Y., Zhang, C., Jiang, Z., Cheng, Y., et al. (2017). Stabilization of Nanoscale Zero-Valent Iron (nZVI) with Modified Biochar for Cr(VI) Removal from Aqueous Solution. *J. Hazard. Mater.* 332, 79–86. doi:10.1016/j.jhazmat.2017.03.002

Donkadokula, N. Y., Kola, A. K., Naz, I., and Saroj, D. (2020). A Review on Advanced Physico-Chemical and Biological Textile Dye Wastewater Treatment Techniques. *Rev. Environ. Sci. Biotechnol.* 19, 543–560. doi:10.1007/s11157-020-09543-z

Gholami, P., Khataee, A., Soltani, R. D. C., Dinpazhoh, L., and Bhatnagar, A. (2020). Photocatalytic Degradation of Gemifloxacin Antibiotic Using Zn-Co-LDH@biochar Nanocomposite. *J. Hazard. Mater.* 382, 121070. doi:10.1016/j.jhazmat.2019.121070

Ghorbani-Khosrowshahi, S., and Behnajady, M. A. (2016). Chromium(VI) Adsorption from Aqueous Solution by Prepared Biochar from Onopordom Heteracanthom. *Int. J. Environ. Sci. Technol.* 13, 1803–1814. doi:10.1007/s13762-016-0978-3

Guo, X., Liu, A., Lu, J., Niu, X., Jiang, M., Ma, Y., et al. (2020). Adsorption Mechanism of Hexavalent Chromium on Biochar: Kinetic, Thermodynamic, and Characterization Studies. *ACS omega* 5, 27323–27331. doi:10.1021/acsomega.0c03652

Huang, X., Hou, X., Song, F., Zhao, J., and Zhang, L. (2016). Facet-Dependent Cr(VI) Adsorption of Hematite Nanocrystals. *Environ. Sci. Technol.* 50, 1964–1972. doi:10.1021/acs.est.5b05111

Ismail, M., Akhtar, K., Khan, M. I., Kamal, T., Khan, M. A., M. Asiri, A., et al. (2019). Pollution, Toxicity and Carcinogenicity of Organic Dyes and Their Catalytic Bio-Remediation. *Cpd* 25, 3645–3663. doi:10.2174/1381612825666191021142026

Jaishankar, M., Tseten, T., Anbalagan, N., Mathew, B. B., and Beeregowda, K. N. (2014). Toxicity, Mechanism and Health Effects of Some Heavy Metals. *Interdiscip. Toxicol.* 7, 60–72. doi:10.2478/intox-2014-0009

Jang, H. M., and Kan, E. (2019). Engineered Biochar from Agricultural Waste for Removal of Tetracycline in Water. *Bioresour. Technol.* 284, 437–447. doi:10.1016/j.biortech.2019.03.131

Jawad, A. H., Mamat, N. F. H., Hameed, B. H., and Ismail, K. (2019). Biofilm of Cross-Linked Chitosan-Ethylene Glycol Diglycidyl Ether for Removal of Reactive Red 120 and Methyl Orange: Adsorption and Mechanism Studies. *J. Environ. Chem. Eng.* 7, 102965. doi:10.1016/j.jece.2019.102965

Jin, J., Sun, K., Liu, W., Li, S., Peng, X., Yang, Y., et al. (2018). Isolation and Characterization of Biochar-Derived Organic Matter Fractions and Their Phenanthrene Sorption. *Environ. Pollut.* 236, 745–753. doi:10.1016/j.envpol.2018.02.015

Jung, K.-W., Kim, K., Jeong, T.-U., and Ahn, K.-H. (2016). Influence of Pyrolysis Temperature on Characteristics and Phosphate Adsorption Capability of Biochar Derived from Waste-Marine Macroalgae (Undaria Pinnatifida Roots). *Bioresour. Technol.* 200, 1024–1028. doi:10.1016/j.biortech.2015.10.016

Kang, S., Kim, G., Choe, J. K., and Choi, Y. (2019). Effect of Using Powdered Biochar and Surfactant on Desorption and Biodegradability of Phenanthrene Sorbed to Biochar. *J. Hazard. Mater.* 371, 253–260. doi:10.1016/j.jhazmat.2019.02.104

Karimi-Maleh, H., Ayati, A., Ghanbari, S., Orooji, Y., Tanhaei, B., Karimi, F., et al. (2021). Recent Advances in Removal Techniques of Cr(VI) Toxic Ion from Aqueous Solution: A Comprehensive Review. *J. Mol. Liq.* 329, 115062. doi:10.1016/j.molliq.2020.115062

Kyzas, G. Z., Siafaka, P. I., Pavlidou, E. G., Chrissafis, K. J., and Bikiaris, D. N. (2015). Synthesis and Adsorption Application of Succinyl-Grafted Chitosan for the Simultaneous Removal of Zinc and Cationic Dye from Binary Hazardous Mixtures. *Chem. Eng. J.* 259, 438–448. doi:10.1016/j.cej.2014.08.019

Li, J., Fan, Q., Wu, Y., Wang, X., Chen, C., Tang, Z., et al. (2016). Magnetic Polydopamine Decorated with Mg-Al LDH Nanoflakes as a Novel Bio-Based Adsorbent for Simultaneous Removal of Potentially Toxic Metals and Anionic Dyes. *J. Mat. Chem. A* 4, 1737–1746. doi:10.1039/c5ta09132b

Liu, S., Wang, W., Cheng, Y., Yao, L., Han, H., Zhu, T., et al. (2020). Methyl Orange Adsorption from Aqueous Solutions on 3D Hierarchical PbS/ZnO Microspheres. *J. Colloid Interface Sci.* 574, 410–420. doi:10.1016/j.jcis.2020.04.057

Lu, Y., Jiang, B., Fang, L., Ling, F., Gao, J., Wu, F., et al. (2016). High Performance NiFe Layered Double Hydroxide for Methyl Orange Dye and Cr(VI) Adsorption. *Chemosphere* 152, 415–422. doi:10.1016/j.chemosphere.2016.03.015

Lustosa Filho, J. F., Penido, E. S., Castro, P. P., Silva, C. A., and Melo, L. C. A. (2017). Co-pyrolysis of Poultry Litter and Phosphate and Magnesium Generates Alternative Slow-Release Fertilizer Suitable for Tropical Soils. *ACS Sustain. Chem. Eng.* 5, 9043–9052. doi:10.1021/acssuschemeng.7b01935

Mahamad, M. N., Zaini, M. A. A., and Zakaria, Z. A. (2015). Preparation and Characterization of Activated Carbon from Pineapple Waste Biomass for Dye Removal. *Int. Biodeterior. Biodegrad.* 102, 274–280. doi:10.1016/j.ibiod.2015.03.009

Mateo-Sagasta, J., Zadeh, S. M., Turral, H., and Burke, J. (2017). Water Pollution from Agriculture: a Global Review. *Exec. Summ*, 35.

Mishra, S., and Bharagava, R. N. (2016). Toxic and Genotoxic Effects of Hexavalent Chromium in Environment and its Bioremediation Strategies. *J. Environ. Sci. Health, Part C* 34, 1–32. doi:10.1080/10590501.2015.1096883

Nguyen, T. H. A., and Oh, S. Y. (2019). Biochar-mediated Oxidation of Phenol by Persulfate Activated with Zero-valent Iron. *J. Chem. Technol. Biotechnol.* 94, 3932–3940. doi:10.1002/jctb.6194

Oh, S.-Y., and Seo, Y.-D. (2016). Sorption of Halogenated Phenols and Pharmaceuticals to Biochar: Affecting Factors and Mechanisms. *Environ. Sci. Pollut. Res.* 23, 951–961. doi:10.1007/s11356-015-4201-8

Pan, Y., Li, Z., Zhang, Z., Tong, X.-S., Li, H., Jia, C.-Z., et al. (2016). Adsorptive Removal of Phenol from Aqueous Solution with Zeolitic Imidazolate Framework-67. *J. Environ. Manag.* 169, 167–173. doi:10.1016/j.jenvman.2015.12.030

Premarathna, K. S. D., Rajapaksha, A. U., Sarkar, B., Kwon, E. E., Bhatnagar, A., Ok, Y. S., et al. (2019). Biochar-based Engineered Composites for Sorptive Decontamination of Water: A Review. *Chem. Eng. J.* 372, 536–550. doi:10.1016/j.cej.2019.04.097

Qiu, Y., Zhang, Q., Gao, B., Li, M., Fan, Z., Sang, W., et al. (2020). Removal Mechanisms of Cr(VI) and Cr(III) by Biochar Supported Nanosized Zero-Valent Iron: Synergy of Adsorption, Reduction and Transformation. *Environ. Pollut.* 265, 115018. doi:10.1016/j.envpol.2020.115018

Shang, T. X., Zhang, J., Jin, X. J., and Gao, J. M. (2014). Study of Cr(VI) Adsorption onto Nitrogen-Containing Activated Carbon Preparation from Bamboo Processing Residues. *J. Wood Sci.* 60, 215–224. doi:10.1007/s10086-014-1392-4

Sun, Y., Yu, I. K. M., Tsang, D. C. W., Cao, X., Lin, D., Wang, L., et al. (2019). Multifunctional Iron-Biochar Composites for the Removal of Potentially Toxic Elements, Inherent Cations, and Hetero-Chloride from Hydraulic Fracturing Wastewater. *Environ. Int.* 124, 521–532. doi:10.1016/j.envint.2019.01.047

Wang, Y., Gao, Y., Chen, L., and Zhang, H. (2015). Goethite as an Efficient Heterogeneous Fenton Catalyst for the Degradation of Methyl Orange. *Catal. Today* 252, 107–112. doi:10.1016/j.cattod.2015.01.012

Wang, Y., Zhang, R., Han, G., and Gao, X. (2020). Band Gap Narrowed P Doped 1T@2H MoS2 Nanosheets towards Synergistically Enhanced Visible Light Photochemical Property. *J. Nanoelectron. Optoelectron.* 15, 257–263. doi:10.1166/jno.2020.2714

Yang, Y., Wang, G., Deng, Q., Ng, D. H. L., and Zhao, H. (2014). Microwave-Assisted Fabrication of Nanoparticulate TiO2 Microspheres for Synergistic Photocatalytic Removal of Cr(VI) and Methyl Orange. *ACS Appl. Mat. Interfaces* 6, 3008–3015. doi:10.1021/am405607h

Yu, J., Zhang, X., Wang, D., and Li, P. (2018). Adsorption of Methyl Orange Dye onto Biochar Adsorbent Prepared from Chicken Manure. *Water Sci. Technol.* 77, 1303–1312. doi:10.2166/wst.2018.003

Zeng, T., Rene, E. R., Zhang, S., and Lens, P. N. L. (2019). Removal of Selenate and Cadmium by Anaerobic Granular Sludge: EPS Characterization and Microbial Community Analysis. *Process Saf. Environ. Prot.* 126, 150–159. doi:10.1016/j.psep.2019.03.039

Zolfi Bavariani, M., Ronaghi, A., and Ghasemi, R. (2019). Influence of Pyrolysis Temperatures on FTIR Analysis, Nutrient Bioavailability, and Agricultural Use of Poultry Manure Biochars. *Commun. Soil Sci. Plant Analysis* 50, 402–411. doi:10.1080/00103624.2018.1563101

Conflict of Interest: The authors declare that the research was conducted in the absence of any commercial or financial relationships that could be construed as a potential conflict of interest.

Publisher's Note: All claims expressed in this article are solely those of the authors and do not necessarily represent those of their affiliated organizations, or those of the publisher, the editors, and the reviewers. Any product that may be evaluated in this article, or claim that may be made by its manufacturer, is not guaranteed or endorsed by the publisher.